High-Performance Thermal Management Nanocomposites: Silver Functionalized Graphene Nanosheets and Multiwalled Carbon Nanotube

Yongcun Zhou[1,2,*], Xiao Zhuang[1], Feixiang Wu[3] and Feng Liu[1,*]

[1] School of Materials Science and Engineering, Northwestern Polytechnical University, Xi'an Shaanxi 710072, P. R. China; yczhou@nwpu.edu.cn (Y.Z.); zhuangxiao@mail.nwpu.edu.cn (X.Z.); liufeng@nwpu.edu.cn (F.L.)

[2] State Key Laboratory of Electrical Insulation and Power Equipment, Xi'an Jiaotong University, Xi'an Shaanxi 710049, P. R. China

[3] Max Planck Institute for Solid State Research, Heisenbergstr. 1, Stuttgart 70569, Germany; F.Wu@fkf.mpg.de (F.W.)

[*] Correspondence: yczhou@nwpu.edu.cn (Y.Z.); liufeng@nwpu.edu.cn (F.L.)；Tel: +86-29-8846-0374 (Y.Z. & F.L.)

Abstract: Silver functionalized graphene nanosheets (GNS) and multiwalled carbon nanotube (MWCNT) composites with excellent thermal properties were developed to meet the requirements of thermal management. The effects of composites on interfacial structure and properties of the composites were identified, and the microstructures and properties of the composites were studied as a function of the volume fraction of fillers. An ultrahigh thermal conductivity of 12.3 W/mK for polymer matrix composites was obtained, which is an approximate enhancement by 69.1 times compared with that of the polyvinyl alcohol (PVA) matrix. Moreover, these composites showed more competitive thermal conductivities compared with those of untreated fillers/PVA composites applied to the desktop central processing unit, making these composites a high-performance alternative to be used for thermal management.

Keywords: Chemical modification; electronics cooling; thermal management nanocomposites; thermal conductivity; silver nanoparticles

1.Introduction

Effective thermal management has become a critical issue to enhance reliability and performance in many research areas including highly integrated electronic devices, lighting components, electronics cooling, and energy-harvesting systems [1-3]. Therefore, it is essential to develop thermal management materials with high thermal conductivity (λ), low coefficient of thermal expansion (CTE), and high insulating property[1,4]. In particular, thermal interface materials (TIM) are typically composed of thermally conductive fillers and viscous polymer matrix to achieve both high thermal conductivity and good frequency stability [1-5]. TIM are essential components for efficient electronics cooling. They act by filling unavoidable air gaps between contacting surfaces of devices and heat sinks. Carbon materials, such as graphene, carbon nanotubes (CNT), graphite, diamond, and carbon fibers (CF), have recently proved to be promising thermal management materials due to their excellent thermal properties [4-7] (graphene high intrinsic λ =5300 W/mK). However, the λ of thermal management nanocomposites was not as high as expected when these various carbon materials were embedded in various polymer matrices because of the presence of an incomplete formation of thermal percolation pathway and large interfacial thermal

resistance (ITR) between fillers and polymer matrix [3-7]. The ITR could become one of the biggest obstacles for heat conduction from good-conducting fillers to poor-conducting polymers.

The ITR in polymer nanocomposites can be classified into filler/matrix resistance and filler/filler resistance [6-14]. Electrically conducting TIM with metal or nano-carbon fillers provided generally higher λ than electrically insulating TIMs with ceramic fillers because additional thermal transport could be realized by electrons [14-17]:

$$\lambda = \lambda_e + \lambda_l = L\sigma T + \lambda_l \qquad (1)$$

where λ_e is the electronic thermal conductivity, λ_l the lattice or phonon thermal conductivity, L the Lorenz number, σ the electrical conductivity, and T the absolute temperature. A significant improvement in σ of polymer matrix or composites has been observed using metal silver (Ag) fillers, nano-carbon, or their combination approaching 40% of intrinsic σ of Ag fillers [18-23].

This study proposed an alternative easy and simple fabrication route, which introduced silver nanoparticles (AgNPs) functionalized graphene nanosheets (GNS) and multiwalled carbon nanotube (MWCNT), forming GNS@AgNPs and MWCNT@AgNPs coating microstructures. (GNS-MWCNT)@AgNPs/PVA flexible film specimens were successfully prepared by introducing the aforementioned structure into a polyvinyl alcohol (PVA) matrix. This combination microstructure was designed to provide an even greater opportunity to enhance λ due to the significantly higher intrinsic λ (about 3000 W/mK) of GNS and MWCNT [23-30] than that of other high–thermal conductivity ceramic fillers, such as AlN and BN. Moreover, AgNPs were chosen because of theirs high thermal conductivity of Ag (λ = 429 W/(mK)) [6,24]. AgNPs functionalized GNS and MWCNT showed a higher σ in functionalized fillers, forming a more effective thermally conductive network and hence lowering the ITR effect. High thermal conductivity and good insulation performance were gained with 20 vf% low filling ratio. This TIM was successfully applied between a heat sink and a central processing unit (CPU) of the computer for efficient cooling. GNS/PVA, MWCNT/PVA, and (GNS-MWCNT)/PVA specimens with the same volume fraction were prepared for comparison.

2. Materials and Methods

1.   2.1. Materials

Ethylene glycol (EG, 99.5%), polyvinyl alcohol (PVA, powder), silver nitrate (AgNO₃, 99.9%), sodium chloride (NaCl, 98%), tetraethylorthosilicate (TEOS, 99.0%), and ammonium hydroxide (NH₄OH, 26 wt%) were purchased from Alfa Aesar Co. (Shanghai, China). Graphene nanosheets (GNS) and multiwalled carbon nanotube (MWCNT) were supplied by Sigma-Aldrich Company (Shanghai, China). Silver (Ag, ~50 nm) nanopowder was supplied by Beijing DK Nano Technology Co. Ltd. (Beijing, China). All other chemical reagents were used as received.

2.   2.2. Characterization

Microstructures and morphologies of the Ag nanoparticles, GNS@AgNPs, and MWCNT@AgNPs were characterized using high-resolution transmission electron microscopy (HRTEM, JEOL JEM-1230, Japan). Scanning electron microscopy (SEM, JEOL 7401F, Japan) was performed with an accelerating voltage of 3 kV, where the samples were sputter-coated with a thin layer of gold for better imaging. The thermal conductivity was measured using a thermal constant analyzer (HOT DISK TPS-2500s, Sweden). The comprehensive thermal analysis with simultaneous differential scanning calorimetry and thermogravimetry (TG) was conducted using a thermal analyzer (NETZSCH STA449C, Germany). The bulk density of the specimen was measured by the water displacement method using an electronic densimeter (METTLER TOLEDO, XPE205, Switzerland). The resistance parameters, including volume resistivity and surface resistivity, were determined using a high-resistance meter (16339, Hewlett Packard, CA, USA) at room temperature. The results were obtained from data average of three samples.

3.   *2.3. Preparation and purification of GNS@AgNPs and MWCNT@AgNPs*

The schematic diagram outlining the preparation of AgNPs functionalized GNS and MWCNT is shown in Figure 1; they were prepared following a previously published protocol with modifications [31-33]. GNS@AgNPs and MWCNT@AgNPs were prepared by the same procedure, which was simple and practical, and could be divided into two parts.
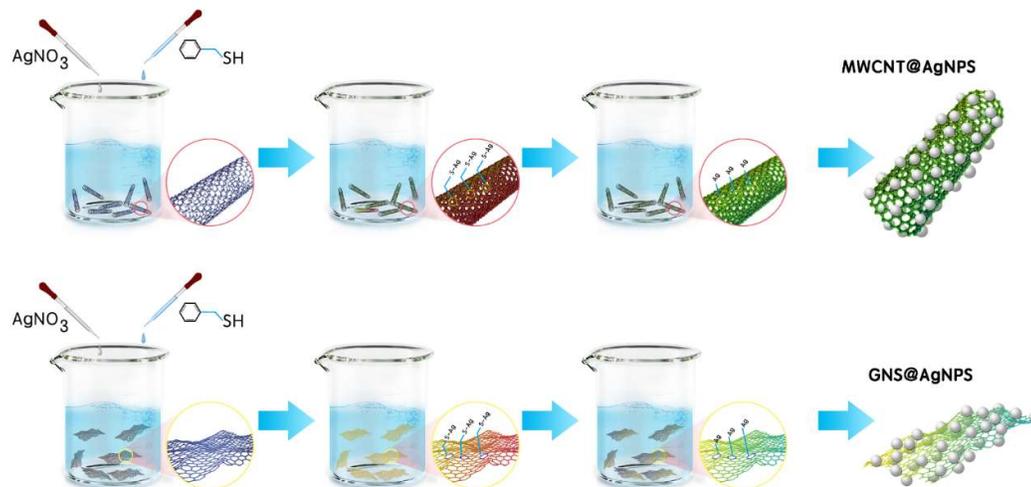
Figure 1. Schematic diagram illustrating the preparation of a coated structure of MWCNT@AgNPs and GNS@AgNPs.

（1）The synthesis of silver nanoparticles was achieved by the sol-gel method. The precursor of silver nanoparticles, silver nitrate solution in 400 mL of ethanol (0.02 mol/L), was stirred with benzyl mercaptan, for about 48 h, and served as a reductant. Hence, silver nanoparticles were successfully synthesized with an average size of about 5 nm and connected with benzyl through the ionic bond with the sulfur ion.

（2）AgNPs and pure ultrasonically dispersed GNS or MWCNT were mixed, stirring for about 30 min, and ultrasonically shaken for about 5 h afterward. Then, they were assembled through benzyl, the cross-linking agent, in which the sulfur ion served as a bridge between silver and benzyl because sulfur has good affinity for silver. Hence, AgNPs adhered to GNS through benzyl. As a result, GNS and MWCNT decorated with AgNPs (GNS@AgNPs and MWCNT@AgNPs, respectively) were obtained after centrifugal separation and drying in a vacuum oven at 60°C for about 12 h.

4.   *2.4. Preparation of GNS@AgNPs/PVA, MWCNT@AgNPs/PVA, and (GNS-MWCNT)@AgNPs/PVA*

The composite film was prepared by the method of tape casting. PVA (3 g) was dissolved in deionized water to a volume of about 60 mL. Then, the dispersed GNS@AgNPs and MWCNT@AgNPs were added into the PVA solution, stirred for about 2 h, and then kept aside for 3 h to remove the bubbles formed during stirring and facilitate the formation of a filler network across AgNPs, which was vital for the thermal conductivity of the composite. The mixture liquid was casted on the plastic film substrate and heated at 60°C. After solidification, the cast layer was separated from the substrate artificially. Ultimately, the PVA matrix nanocomposite containing hybrid GNS@AgNPs and MWCNT@AgNPs fillers was successfully obtained.

3. Results and Discussion

The SEM and TEM images of core-shell GNS@AgNPs and MWCNT@AgNPs are shown in Figure 2. As shown in Figure 2a, AgNPs were uniformly attached on the surface of microscale GNS. Figure 2b shows the TEM image of AgNPs; their size was about 20 nm. Also, the silver lattice constant was about 0.23 nm, as shown in Figure 2d. Similarly, AgNPs were uniformly attached to the

surface of MWCNT, as shown in Figure 2c. The silver diffraction pattern is shown in the inset of Figure 2c.
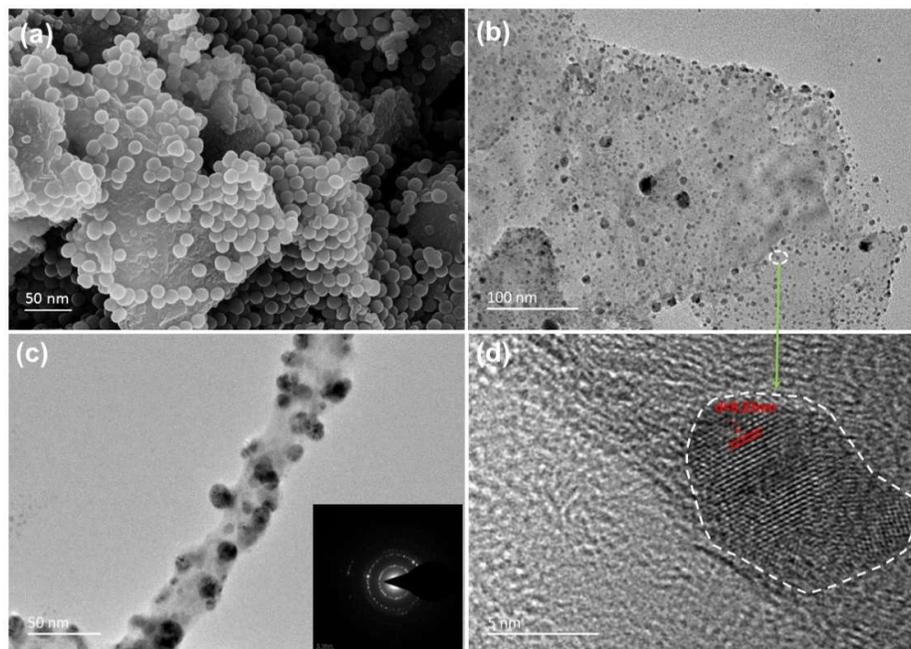
Figure 2. (a) SEM image of GNS@AgNPs and (b) TEM image of GNS@AgNPs. (c) TEM image of MWCNT@AgNPs. (d) Partially enlarged structures of (b). The lattice constant *d* of silver was 0.23 nm. The silver lattice diffraction pattern is shown in the inset of (c).

The surface modification of GNS nanosheets and MWCNT by AgNPs provided hydroxyl groups on the surface of nanoparticles, improving the distribution of GNS-MWCNT in the PVA polymer matrix. The thermal properties of the composite films are summarized in Table 1. The glass transition temperature (T_g) of the composite films was higher than that of the neat PVA, indicating that the nanofillers increased the T_g of the PVA matrix. The neat PVA exhibited high thermal oxidation stability. The thermo-oxidative decomposition behavior of the PVA nanocomposites was similar to that of PVA but showed a higher decomposition temperature, suggesting that the addition of (GNS-MWCNT)/AgNPs improved the thermal stability of the PVA nanocomposites. The CTE of the PVA composite films decreased with the increasing concentration of nanofillers. Thus, a substantial decrease in the CTE of PVA films originated from adequate dispersion and interfacial physical bonds between the nanofillers and the PVA matrix. The nanofillers prevented the mobility of the loose molecular bonds in polymer chains with increasing temperature [33-39]. For the composite films, CTE is dependent on each component phase and the interactions between each phase. Hence, the substantial decrease in CTE of PVA films should originate from the adequate dispersion and interfacial physical bonds between the nanofillers and the PVA matrix. The nanofiller can restrain the mobility of the loose molecular bonds in polymer chains as the temperature increases.

Both the volume and surface resistance of the (GNS-MWCNT)@AgNPs/PVA composite films with different volume fractions of fillers (0, 5%, 10%, 15%, and 20%) were measured at room temperature. The results are presented in Figure 3. As shown in Figure 3, the volume and surface resistance of the films decreased gradually with increased nanofiller loading. The results suggested that although the volume resistance and surface resistance of the films decreased gradually, they were within the range of accepted properties for electronic packaging and/or electrical insulation material applications [26,40-45].
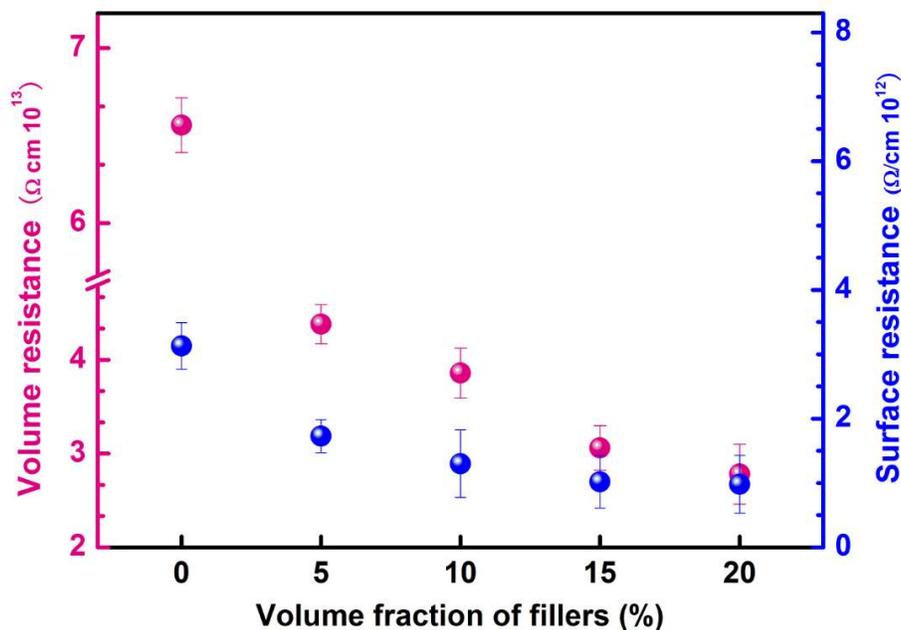
Figure 3. Effect of filler loading on volume resistance and surface resistance of (GNS-MWCNT)@AgNPs/PVA nanocomposite films.

Table 1. Glass transition temperatures, coefficient of thermal expansion, and thermal decomposition temperature of neat PVA and its composites filled with GNS, MWCNT, and (GNS-MWCNT)@AgNPs at 5, 10, 15, and 20% fillers loading.

Sample	Content (vol%)	T_g^a (ºC)	CTE^b (ppm/ ºC)	$T_{d5\%}^c$ (ºC)
Neat PVA	0	210.8±5.4	40.5±1.2	517.3±10.4
GNS/PVA	5	211.4±6.3	40.1±1.6	525.6±11.2
	10	211.6±4.2	39.5±2.4	517.5±9.80
	15	211.8±6.1	38.4±2.3	528.2±10.8
	20	211.3±5.3	38.2±2.1	527.3±10.3
MWCNT/PVA	5	210.5±5.8	39.5±3.0	514.3±9.90
	10	211.3±4.9	39.4±2.7	513.5±11.2
	15	211.4±4.1	38.8±2.6	528.2±10.8
	20	211.6±5.6	38.2±2.7	522.9±12.3
(GNS-MWCNT)@AgNPs /PVA	5	210.4±6.1	39.8±2.2	518.2±11.1
	10	210.5±4.8	39.5±3.2	519.4±10.2
	15	211.2±6.5	38.7±3.3	524.8±10.9
	20	211.4±5.5	38.2±2.8	526.2±11.4

T_g^a, glass transition temperature. CTE^b, coefficient of thermal expansion, measured using TMA determined over a range of 100ºC–200ºC. $T_{d5\%}^c$, thermal decomposition temperature at 5% weight loss as determined using TGA.

The thermal conductivities of composites greatly depended on the properties of polymers and fillers, such as their content, components, and surface treatment of fillers [46-50]. Comparison charts of thermal conductivities and their enhancements for GNS/PVA, MWCNT/PVA, (GNS-MWCNT)/PVA, and (GNS-MWCNT)@AgNPs/PVA composite films with different nanofillers are shown in Figure 4. As shown in Figure 4a, the thermal conductivity of the pure PVA was about 0.178 W/mK. The thermal conductivities of the aforementioned four composite films increased with the increase in filler loading. Further, the thermal conductivity of (GNS-MWCNT)@AgNPs/PVA was higher than that of the other three films and reached the highest value of 12.3W/mK at 20% filler

loading. The efficiency of fillers in thermally conductive materials was characterized by thermal conductivity enhancement, which was defined by the following equation [48]:

$$\eta\ (\%) = \frac{K - K_m}{K_m} \times 100 \tag{2}$$

where K represents the thermal conductivity of the composite, and K_m is the thermal conductivity of the matrix material. As shown in Figure 4b, the enhanced matrix thermal conductivity was always larger than that for GNS/PVA, MWCNT/PVA, and (GNS-MWCNT)/PVA composite films at 5%, 10%, 15%, and 20% filler loading, respectively. The maximum thermal conductivity of (GNS-MWCNT)@AgNPs/PVA composite with 20% filler low loading increased to 12.3 W/mK, representing an approximate enhancement of 6810.1 times compared with that of the used neat PVA matrix. Graphene nanosheets could be considered as a 2D materials, multiwalled carbon nanotube could be considered as a one-dimensional material, and GNS@AgNPs and MWCNT@AgNPs could be considered as 2@0 and 1@0 coated structures. Compared with GNS/PVA and MWCNT/PVA films, silver nanoparticles coated with GNS and MWCNT provided an effective bond between fillers and PVA polymer, enabling effective thermal conductivity compared with that of films without silver nanoparticles at the same filler loading. Hence, it was fair to conclude that multidimensional structure fillers improved the thermal conductivity of polymer matrix composite materials compared with the single-dimensional structure fillers. [28]
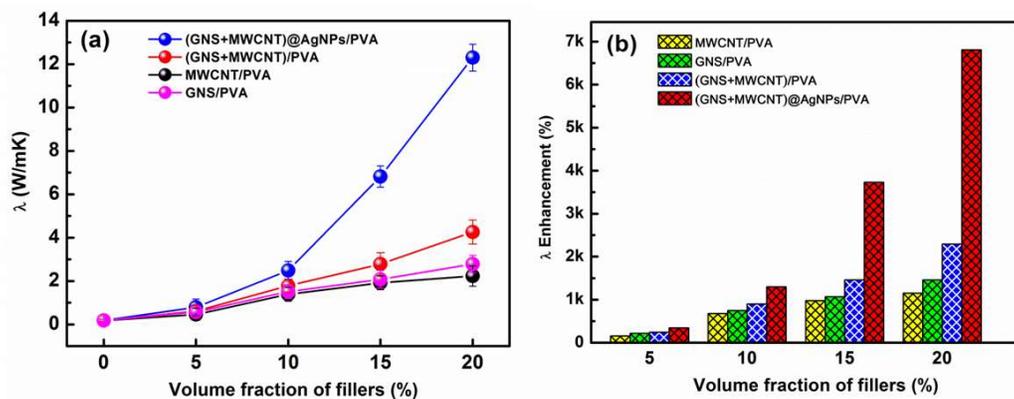
Figure 4. Thermal conductivity λ (a) and thermal conductivity enhancement (b) of GNS/PVA, MWCNT/PVA, (GNS-MWCNT)/PVA, and (GNS-MWCNT)@AgNPs/PVA nanocomposite films with different volume fractions of fillers.

Printability and thermal expansion are important parameters of TIM when applied between the surfaces of heat-generating devices and heat sink in the advanced microelectronics packaging technology. The CPU cooling of the desktop computer was investigated using TIM for heat dissipation, as shown in Figure 5a. The (GNS-MWCNT)@AgNPs/PVA TIM was applied between the CPU and a heat sink and cured at 120°C for 5 h. A cooler master fan was attached at the top of the heat sink. The surface temperature of the CPU (T_{CPU}) was measured using T-type thermocouples at room temperature. A commercial TIM (ARCTIC MX-4, Shenzhen, China λ=8.5 W/mK) was chosen as a comparison. As shown in Figure 5b, T_{CPU} without and with two kinds of TIMs were room temperature initially, which increased gradually with the increase in time. T_{CPU} without TIM was more than 50°C after about 2000 seconds and increased with time, gradually into the abnormal conditions (more than 50°C). However, T_{CPU} with two kinds of TIMs were always normal, a better heat dissipation performance was obtained by the (GNS-MWCNT)@AgNPs/PVA TIM compared with that of commercial TIM. The highest T_{CPU} of (GNS-MWCNT)@AgNPs/PVA TIM was only about 40°C. Hence, it was evident that using TIM obtained could more effectively reduce the redundant heat compared with CPU without TIM and commercial TIM.
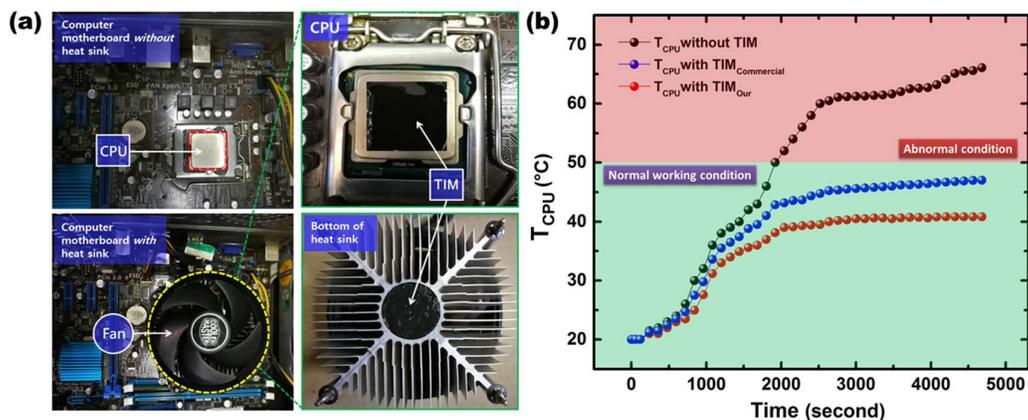
Figure 5. Changes in computer CPU cooling with the temperature of (GNS-MWCNT)@AgNPs/PVA TIM and a commercial TIM were investigated. An optical image of the coating-printed (GNS-MWCNT)@AgNPs/PVA TIM is provided in the inset of (a). Optical images of a CPU on a motherboard before and after the installation of a heat sink with a fan. T-type thermocouples were employed to measure the temperatures of the CPU. Temperature (T_{CPU}) profiles were investigated with two kinds of TIMs and without TIM between the CPU and heat sink. (b) Experimental data of T_{CPU} with TIMs under normal working conditions were also compared with the data of T_{CPU} without TIM.

4. Conclusions

In summary, silver-functionalized GNS and MWCNT composites with excellent thermal properties were developed in this study. The effects of composites on the interfacial structure and properties of the composites were identified, and the microstructures and properties of the composites were studied as a function of the volume fraction of fillers. An ultrahigh thermal conductivity of 12.3 W/mK for polymer matrix composites was obtained, which was enhanced by approximately 69.1 times compared with that of the PVA matrix. Further, these composites displayed more competitive thermal conductivities compared with that of untreated fillers/PVA composites, making these composites a high-performance alternative to be used for thermal management or electronics cooling.

Authors Contributions: Y.Z. and X.Z. designed and performed all experiments. Y.Z. and F.W. analyzed the data and wrote the manuscript. All authors have read and approved the final manuscript.

Funding: This study was supported by the National Natural Science Foundation of China (51707159), the Natural Science Foundation of Shannxi Province (2017JM5073), the State Key Laboratory of Electrical Insulation and Power Equipment (EIPE17205), and the Fundamental Research Funds for the Central Universities (3102017zy047).

Conflicts of Interest: The authors declare no conflicts of interest.

References

1. De Volder, M.F.L.; Tawfick, S.H.; Baughman, R.H.; Hart, A.J. Carbon nanotubes: Present and future commercial applications. *Science* **2013**, *339*, 535-539.
2. Chen, J; Huang, X.; Zhu, Y.; Jiang, P. Cellulose Nanofiber Supported 3D Interconnected BN Nanosheets for Epoxy Nanocomposites with Ultrahigh Thermal Management Capability. *Adv. Funct. Mater.* **2017**, *27*, 1604754.
3. Fu, Z.; Chen, K.; Li, L.; Zhao, F.; Wang, Y.; Wang, M.; Shen, Y.; Cui, H.; Liu, D.; Guo, X. Spherical and spindle-like abamectin-loaded nanoparticles by flash nanoprecipitation for southern root-knot nematode control: preparation and characterization. *Nanomaterials* **2018**, *8*, 449.

4. Wang, G.; Yu, D.; Kelkar, A.D.; Zhang, L. Electrospun nanofiber: emerging reinforcing filler in polymer matrix composite materials. *Prog. Polym. Sci.* **2017,** *75*, 73-107.
5. Wang, Y.; Wang, A.; Wang, C.; Cui, B.; Sun, C.; Zhao, X.; Zeng, Z.; Shen, Y.; Gao, F.; Liu, G.; et al. Synthesis and characterization of emamectin-benzoate slow-release microspheres with different surfactants. *Sci. Rep.* **2017,** *7*, 12761.
6. Shen, Y.; Wang, Y.; Zhao, X.; Sun, C.; Cui, B.; Gao, F.; Zeng, Z.; Cui, H. Preparation and physicochemical characteristics of thermo-responsive emamectin benzoate microcapsules. *Polymers* **2017,** *9*, 418.
7. Zhou, Y.; Yao, Y.; Chen, C.; Moon, K.; Wang, H.; Wong, C.P. The use of polyimide-modified aluminum nitride fillers in AlN@PI/Epoxy composites with enhanced thermal conductivity for electronic encapsulation. *Sci. Rep.* **2014,** *4*, 4779.
8. Pan, C.; Zhang, J.; Kou, K.; Zhang, Y.; Wu, G. Investigation of the through-plane thermal conductivity of polymer composites with in-plane oriented hexagonal boron nitride. *Int. J. Heat Mass Transf.* **2018,** *120*, 1-8.
9. Saadah, M.; Hernandez, E.; Balandin, A. Thermal Management of Concentrated Multi-Junction Solar Cells with Graphene-Enhanced Thermal Interface Materials. *Appl. Sci.* **2017,** *7*, 589.
10. Li, Z.; Li, Z.; Sun, S.; Zheng, D.; Wang, H.; Tian, H.; Yang, H.; Bai, X.; Li, J. Direct observation of inner-layer inward contractions of multiwalled boron nitride nanotubes upon in situ heating. *Nanomaterials* **2018,** *8*, 86.
11. Wang, J.; Wang, H.; Cao, D.; Lu, X.; Han, X.; Niu, C. Epitaxial growth of urchin-like $CoSe_2$ nanorods from electrospun co-embedded porous carbon nanofibers and their superior lithium storage properties. *Part. Part. Syst. Charact.* **2017,** *34*, 1700185.
12. Feng, A.; Jia, Z.; Yu, Q.; Zhang, H.; Wu, G. Preparation and characterization of carbon nanotubes/carbon fiber/phenolic composites on mechanical and thermal conductivity properties. *NANO* **2018,** *13*, 1850037.
13. Renteria, J.; Legedza, S.; Salgado, R.; Balandin, M.P.; Ramirez, S.; Saadah, M.; Kargar, F.; Balandin, A.A. Magnetically-functionalized self-aligning graphene fillers for high-efficiency thermal management applications. *Mater. Des.* **2015,** *88*, 214-221.
14. Cavallaro, G.; Danilushkina, A.A.; Evtugyn, V.G.; Lazzara, G.;Milioto, S.; Parisi, F.; Parisi, E.V.; Fakhrullin, R.F. Halloysite nanotubes: controlled access and release by smart gates. *Nanomaterials* **2017,** *7*, 199.
15. Zhou, Y.C.; Wang, H.; Wang, L.; Yu, K.; Lin, Z.D.; Bai, Y.Y. Fabrication and characterization of aluminum nitride polymer matrix composites with high thermal conductivity and low dielectric constant for electronic packaging. *Mater. Sci. Eng. B* **2012,** *177*,892-896.
16. Zhou, Y.C.; Wang, H.; Xiang, F.; Zhang, H.; Yu, K.; Chen, L. A poly(vinylidene fluoride) composite with added self-passivated microaluminum and nanoaluminum particles for enhanced thermal conductivity. *Appl. Phys. Lett.* **2011,** *98*, 182906.
17. Yu, L.; Park, J.; Lim, Y.; Lee, C.; Shin, K.; Moon, H.; Yang, C.; Lee, Y.; Han, J. Carbon hybrid fillers composed of carbon nanotubes directly grown on graphene nanoplatelets for effective thermal conductivity in epoxy composites. *Nanotechnology* **2013,** *24*,155604.
18. Terao, T.; Zhi, C.; Bando, Y.; Mitome, M.; Tang, C.; Golberg, D. Alignment of boron nitride nanotubes in polymeric composite films for thermal conductivity improvement. *J. Phys. Chem. C* **2010,** *114*, 4340–4344.
19. Zhao, Y.; Zhang, Y.; Bai, S. High thermal conductivity of flexible polymer composites due to synergistic effect of multilayer graphene flakes and graphene foam. *Compos. Part A* **2016,** *85*, 148–155.
20. Wang, F.; Drzal, L.T.; Qin, Y.; Huang, Z. Enhancement of fracture toughness, mechanical and thermal properties of rubber/epoxy composites by incorporation of graphene nanoplatelets. *Compos. Part A* **2016,** *87*, 10–22.
21. Shenogin, S.; Bodapati, A.; Xue, L.; Ozisik, R.; Keblinski, P. Effect of chemical functionalization on thermal transport of carbon nanotube composites. *Appl. Phys. Lett.* **2004,** *85*, 2229-2231.
22. Guo, K.; Hu, Z.; Song, H.; Du, X.; Zhong, L.; Chen, X. Low-density graphene/carbon composite aerogels prepared at ambient pressure with high mechanical strength and low thermal conductivity. *RSC Adv.* **2015,** *5*, 5197-5204.
23. Fan, Z.; Tng, D.Z.Y.; Nguyen, S.T.; Feng, J.D.; Lin, C.F.; Xiao, P.F.; Lu, L.; Duong, H.M. Morphology effects on electrical and thermal properties of binderless graphene aerogels. *Chem. Phys. Lett.* **2013,** *561*, 92-96.
24. Cheng, Y.; Zhou, S.; Hu, P.; Zhao, G.; Li, Y.; Zhang, X.; Han, W. Enhanced mechanical, thermal, and electric properties of graphene aerogels via supercritical ethanol drying and high-temperature

thermal reduction. *Sci. Rep.* **2017,** *7*, 1439.

25. Gong, F.; Bui, K.; Papavassiliou, D.V.; Duong, H.M. Thermal transport phenomena and limitations in heterogeneous polymer composites containing carbon nanotubes and inorganic nanoparticles. *Carbon* **2014,** *78*, 305-316.

26. Deng, Y.; Li, J.H.; Nian, H.G.; Li, Y.L.; Yin, X.P. Design and preparation of shape-stabilized composite phase change material with high thermal reliability via encapsulating polyethylene glycol into flower-like TiO₂, nanostructure for thermal energy storage. *Appl. Therm. Eng.* **2017,** *114*, 328-336.

27. Roy, A.K.; Farmer, B.L.; Varshney, V.; Sihn, S.; Lee, J.; Ganguli, S. Importance of interfaces in governing thermal transport in composite materials: Modeling and experimental perspectives. *ACS Appl. Mater. Interfaces* **2012,** *4*, 545-563.

28. Zhou, Y.; Liu, F.; Wang, H. Novel organic-inorganic composites with high thermal conductivity for electronic packaging applications: A key issue review. *Polym. Compos.* **2017,** *38*, 803-813.

29. Safari, A.; Saidur, R.; Sulaiman, F.A.; Xu, Y.; Dong, J. A review on supercooling of Phase Change Materials in thermal energy storage systems. Renew. *Sustain. Energy Rev.* **2016,** *70*, 905-919.

30. Zhou, Y.; Liu, F. High-performance polyimide nanocomposites with core-shell AgNWs@BN for electronic packagings, *Appl. Phys. Lett.* **2016,** *109*, 082901.

31. Su, J.F.; Wang, X.Y.; Han, S.; Zhang, X.L.; Guo, Y.D.; Wang, Y.Y.; Tan, Y.Q. Preparation and physicochemical properties of microcapsules containing phase change material with graphene/organic hybrid structure shells. *J. Mater. Chem. A* **2017,** *5*, 23937-23951.

32. Cai, Y.; Sun, G.; Liu, M.; Zhang, J.; Wang, Q.; Wei, Q. Fabrication and characterization of capric-lauric-palmitic acid/electrospun SiO₂, nanofibers composite as form-stable phase change material for thermal energy storage/retrieval. *Sol. Energy* **2015,** *118*, 87-95.

33. Chun, K.Y.; Oh. Y.; Rho, J.; Ahn, J.H.; Kim, Y.J.; Choi, H.; Baik, S. Highly conductive, printable and stretchable composite films of carbon nanotubes and silver. *Nature nanotech.* **2010,** *5*, 853-857.

34. Zhang, X.; Sun, D.; Li, Y.; Lee, G.-H.; Cui, X.; Chenet, D.; You, Y.; Heinz, T.F.; Hone, J.C. Measuremen of Lateral and Interfacial Thermal Conductivity of Single- and Bilayer MoS₂ and MoSe2 Using Refined Optothermal Raman Technique. *ACS Appl. Mater. Interfaces* **2015,** *7*, 25923-25929.

35. Zhao, Y.J.; Min, X.; Huang, Z.H.; Fang, M.H. Honeycomb-like structured biological porous carbon encapsulating PEG: A shape-stable phase change material with enhanced thermal conductivity for thermal energy storage. *Energy Build.* **2017,** *158*, 1049-1062.

36. Ibrahim, N.I.; Al-Sulaiman, F.A.; Rahman, S.; Yilbas, B.S.; Sahin, A.Z. Heat transfer enhancement of phase change materials for thermal energy storage applications: A critical review. Renew. *Sustain. Energy Rev.* **2017,** *74*, 26-50.

37. Lv, P.Z.; Liu, C.Z.; Rao, Z.H. Review on clay mineral-based form-stable phase change materials: Preparation, characterization and applications. Renew. *Sustain. Energy Rev.* **2016,** *68*, 707-726.

38. Bauld, R.; Choi, D.Y.W.; Bazylewski, P.; Divigalpitiya, R.; Fanchini, G. Thermo-optical characterization and thermal properties of graphene-polymer composites: A review. *J. Mater. Chem. C* **2018,** *6*, 2901-2914.

39. Zhang, L.; Yang, W.B.; Jiang, Z.N.; He, F.F.; Zhang, K.; Fan, J.H.; Wu, J.Y. Graphene oxide-modified microencapsulated phase change materials with high encapsulation capacity and enhanced leakage-prevention performance. *Appl. Energy* **2017,** *197*, 354-363.

40. Su, J.F.; Wang, L.X.; Ren, L.; Huang, Z. Mechanical properties and thermal stability of double-shell thermal energy storage microcapsules. *J. Appl. Polym. Sci.* **2007,** *103*, 1295-1302.

41. Wang, J.J.; Yang, M.; Lu, Y.F.; Jin, Z.K.; Tan, L.; Gao, H.Y.; Fan, W.J.; Wang, G. Surface functionalization engineering driven crystallization behavior of polyethylene glycol confined in mesoporous silica for shape-stabilized phase change materials. *Nano Energy* **2016,** *19*, 78-87.

42. Wang, F.F.; Zeng, X.L.; Yao, Y.M.; Sun, R.; Xu, J.B.; Wong, C.P. Silver Nanoparticle-Deposited Boron Nitride Nanosheets as Fillers for Polymeric Composites with High Thermal Conductivity. *Sci. Rep.* **2016,** *6*, 19394.

43. Zhuang, X.; Zhou. Y.C.; Liu, F. A novel 3D sandwich structure of hybrid graphite nanosheets and silver nanowires as fillers for improved thermal conductivity. *Mater. Res. Express* **2017,** *4*, 015018.

44. Zhou, Y.C.; Luo, Z.P.; Zhuang, X.; Liu, F. Multilayer-structured high-performance nanocomposites based on a combination of silver nanoparticles and nanowires. *Mater. Lett.* **2016,** *182*, 323-327.

45. Zhou, Y.C.; Wang, H.; Wang, L.; Yu, K.; Lin, Z.D.; Bai, Y.Y. Fabrication and characterization of aluminum nitride polymer matrix composites with high thermal conductivity and low dielectric constant for electronic packaging. *Mater. Sci. Eng. B* **2012,** *177*,892-896.

46. Zhou, Y.C.; Wang, H.; Xiang, F.; Zhang, H.; Yu, K.; Chen, L. A poly(vinylidene fluoride) composite

with added self-passivated microaluminum and nanoaluminum particles for enhanced thermal conductivity. *Appl. Phys. Lett.* **2011,** *98*, 182906.

47. Dong, Q.; Yoon, S.J.; Zhang, J.; Yoon, H.S.; Kim, T.G. Research on Thermal Conductivity of Electrospun Polyacrilonitrile-Multi-Walled Carbon Nanotubes Composite Carbon Nanofiber Papers. *J. Nanosic. Nanotechno.* **2018,** *18*, 7095-7099.

48. Zhang, X.; Tan, W.; Smail, F.; De Volder, M.; Fleck, N.; Boies, A. High-fidelity characterization on anisotropic thermal conductivity of carbon nanotube sheets and on their effects of thermal enhancement of nanocomposites. *Nanotechnology* **2018,** *29*, 365708.

49. Sadej, M.; Gojzewski, H.; Gajewski, P.; Vancso, G.J.; Andrzejewska, E. Photocurable acrylate-based composites with enhanced thermal conductivity containing boron and silicon nitrides. *Express Polym. Lett.* **2018,** *12*, 790-807.

50. Xu, Y.J.; Ren, S.X.; Zhang, W.H. Thermal conductivities of plain woven C/SiC composite: Micromechanical model considering PyC interphase thermal conductance and manufacture-induced voids. *Compos. Struct.* **2018,** *193*, 212-223.